energies

MDPI

Article

Effect of MXene Loaded on g-C_3N_4 Photocatalyst for the Photocatalytic Degradation of Methylene Blue

Muhammad Syahmi Irfan Nasri [1], Mohamad Fakhrul Ridhwan Samsudin [1,*], Asif Ali Tahir [2,*] and Suriati Sufian [1,3,*]

[1] Chemical Engineering Department, Universiti Teknologi PETRONAS, Bandar Seri Iskandar 32610, Perak, Malaysia; msyahmiirfan96@gmail.com
[2] Environment and Sustainability Institute, University of Exeter, Penryn TR10 9FE, Cornwall, UK
[3] Centre of Innovative Nanostructures & Nanodevices (COINN), Universiti Teknologi PETRONAS, Bandar Seri Iskandar 32610, Perak, Malaysia
* Correspondence: mohamadfakhrulridhwan@gmail.com (M.F.R.S.); a.tahir@exeter.ac.uk (A.A.T.); suriati@utp.edu.my (S.S.)

Abstract: Photocatalytic degradation is one of the environmentally friendly methods used in treating dye wastewater. In this study, a series of MXene/g-C_3N_4 heterostructure photocatalysts with different loading amounts of MXene (1, 4, 8, and 12 wt.%) were successfully synthesized via the wet impregnation method and their photocatalytic activity was evaluated via the degradation of methylene blue under visible-light irradiation. As such, the 1 wt.% MXene/g-C_3N_4 heterostructure photocatalyst achieved a high degradation of methylene blue compared to the pure g-C_3N_4 under visible-light illumination of 180 min. This significant improvement was attributed to the intimate interfacial contact, evidently from the FESEM analysis, which allows the smooth photocharge carriers to transport between g-C_3N_4 and MXene. Additionally, the larger BET surface area demonstrated by the 1 wt.% MXene/g-C_3N_4 heterostructure allowed this sample to have higher adsorption of dye molecules and provided a higher number of reactive sites, which was beneficial for the enhancement of the photocatalytic activity. Nevertheless, it was found that the excessive loading of MXene can substantially impede photocatalytic activity. This was attributed to the decrease in the active sites, as well as the weakened crystallinity of the MXene/g-C_3N_4 heterostructure photocatalyst, evident from the FTIR and XRD analysis. All in all, this study has shown the potential of the MXene/g-C_3N_4 photocatalyst as a promising photocatalyst for highly efficient wastewater treatment applications.

Keywords: graphitic carbon nitride; MXene; degradation; methylene blue; wastewater

Citation: Nasri, M.S.I.; Samsudin, M.F.R.; Tahir, A.A.; Sufian, S. Effect of MXene Loaded on g-C_3N_4 Photocatalyst for the Photocatalytic Degradation of Methylene Blue. *Energies* **2022**, *15*, 955. https://doi.org/10.3390/en15030955

Academic Editor: Valerio Lo Brano

Received: 17 October 2021
Accepted: 28 December 2021
Published: 28 January 2022

1. Introduction

Nowadays, the textile industry has proven to be one of the most important industries to humankind as clothes serve as a basic need for humans. The textile industry has grown rapidly over recent years, contributing 7% of total world exports worth US $1 trillion and employing 35 million people around the globe [1]. However, the textile industry poses a serious environmental issue as it consumes a huge amount of fresh water on a daily basis and discharges 0.7 megatons of dyes products annually [2]. The released colored dye can cause several environmental issues, such as contamination of viable water sources, as well as endangering aquatic life and eventually causing harm to the human society if not controlled. Methylene blue (MB) can be commonly found inside dye waste and its natural composition is highly carcinogenic due to the presence of aromatic compounds and amines, resulting in histamine poisoning [3].

In recent years, various methods for wastewater treatment, especially for methylene blue, such as adsorption, sedimentation, filtration through a membrane, and coagulation, has been explored [4]. Even though these methods can remove most pollutants, research has also showed that the pollutants were not fully eliminated [5]. Other than that, the

aforementioned environmental technologies are not very efficient for this purpose as they demand high chemical and operational costs, generation of complex sludge, and need a long time to work. It is important to explore new alternatives that are able to further degrade methylene blue with low-cost materials, as well as minimize the energy required. AOP (advanced oxidation process) is one of the viable options and is a propitious wastewater treatment activity, capable of degrading most of the pollutants as the as-generated hydroxyl radicals possess high oxidation prospects [6].

Photocatalysis is one of the applications of an advanced oxidation process, utilizing solar energy to initiate the reaction, and has become a very favorable method in treating the water pollution issues due to its sustainability and eco-friendly attributes [7]. Graphitic carbon nitride (g-C_3N_4) has been a promising candidate in the photocatalytic arena as it has high thermal and chemical durability, moderate bandgap energy (~2.7 eV), non-toxicity, is economical, and has a high surface area for the reaction [8]. However, the performance of g-C_3N_4 upon photocatalytic reaction has been limited due to its high recombination of photogenerated electrons and holes [9]. Therefore, it is very crucial for a subsequent treatment to further improve the photocatalytic reaction of pristine g-C_3N_4. In recent years, various strategies for the improvement of g-C_3N_4 have been proposed, such as structural modifying, improving crystallized structure, combining with a different photocatalyst that has an appropriate band edge position, and loading with a co-catalyst [10]. Among the aforementioned strategies, loading the g-C_3N_4 with different photocatalyst material for the formation of the heterostructure system has shown promise in expediting the separation of the photocharge carrier with respect to the formation of the Schottky junction [11].

MXene, a new type of 2D transition metal carbide, nitride, or carbonitride, which is obtained by etching the Ti_3AlC_2, has caught significant attention as a coupled photocatalyst material for the formation of the heterostructure system. This is attributed to its peculiar features, including excellent stability in structure, a large number of hydrophilic functional groups on its surface, great metal conductivity, and stronger redox reactivity stemming from its surface terminal Ti sites [12]. In light of this, MXene has abundant surface groups and huge exposed metal sites, which enable strong annexation with 2D photocatalyst, making it an efficient co-catalyst to expedite photocatalytic degradation of methylene blue [13,14]. With respect to the abovementioned intriguing features of MXene, it is expected that the combination of MXene and g-C_3N_4 photocatalyst can further enhance the photocatalytic activity of the g-C_3N_4 photocatalyst. In addition, encouraged by the advantages of MXene, which possesses an excellent metallic conductivity, the formation of the aforesaid heterostructure system will induce the development of a Schottky junction, which results in the formation of a built-in electric field. Thereinto, this phenomenon is greatly known to significantly improve the photocharge carriers' separation and migration within the heterostructure system, resulting in an augmentation in photocatalytic degradation performance.

Sparked by this inspiration, in the present work, the formation of g-C_3N_4/MXene heterostructure photocatalyst with Schottky junction was synthesized via a wet-impregnation method. The performance of the aforesaid heterostructure photocatalyst was evaluated using the degradation of methylene blue. Moreover, several characterization techniques were used in order to examine the properties of the designed photocatalyst, including XRD, FTIR, SAP, XPS, FESEM, HRTEM, and DR-UV-Vis analysis. The obtained photocatalyst composite presents a notable improvement in photocatalytic degradation of methylene blue. The improved photodegradation can be associated with the harmony effect of the Schottky junction formed, as well as the 2D/2D interfacial contact between both materials, enhancing the efficiency for separation and mobility of the photocharge carriers for photocatalytic reaction. On a whole, this work opens up an invigorating avenue for wastewater treatment applications, particularly on the removal of dye, in which this work offers highly efficient photocatalyst materials to be used with excellent performance.

2. Materials and Methods

2.1. Materials

All of the reagents and solutions used to synthesize photocatalysts and photocatalytic degradation studies were of analytical grade and were used without any further purification. Urea (purity of 99%), hydrofluoric acid (assay at 49%), Ti_3AlC_2 (purity of 90%), and methylene blue powder were purchased from Sigma-Aldrich company (St. Louis, MO, USA). The deionized water was used in preparing all required aqueous solutions during the experiments.

2.2. Photocatalyst Preparation

The g-C_3N_4 was synthesized using thermal polycondensation of urea by adopting a method from the previous article [15]. Alumina crucible was filled with urea powder until it reached $^3/_4$ of the crucible, followed by constant heating in a furnace for 120 min at 500 °C with a heating rate of 5 °C/min. After the completion of the reaction, the furnace was left to cool down to room temperature. The green-yellowish powder accumulated inside the crucible was collected and crushed with a mortar.

The formation of MXene was conducted via a chemical etching process according to the reported literature [16]. At room temperature, 1 g of Ti_3AlC_2 was mixed with 10 mL of 49% HF while slowly stirring the solution for 24 hrs. The precipitate of the etched formate was collected and washed with deionized water and centrifuged until the pH value was close to 7. The moisture of the black powder was removed by letting it dry in the oven at 60 °C overnight.

The composites of MXene/g-C_3N_4 heterostructure photocatalysts were synthesized by using the wet impregnation method, as shown in Figure 1. Initially, 1 g of g-C_3N_4 was added with 0.01 g MXene (labelled as 1 wt.% MXene/g-C_3N_4) and 30 mL of deionized water. The mixture then underwent sonication for 30 min at room temperature. Then, the mixture was stirred with heat for 45 min until a slurry was formed. The sample was left to dry in the oven with a temperature of 60 °C for overnight drying. The sample was then collected in a vial. The steps were repeated for the composites labelled as 4, 8, and 12 wt.% MXene/g-C_3N_4 by changing the weight of MXene to 0.04, 0.08, and 0.12 g, respectively.

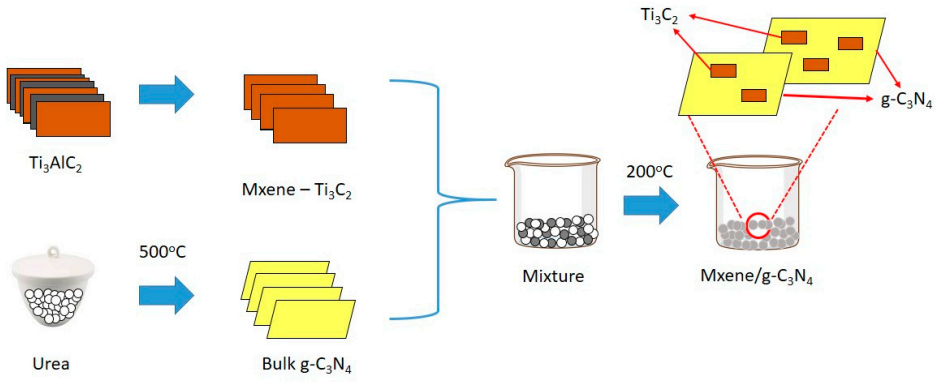

Figure 1. Schematic diagram of the MXene/g-C_3N_4 photocatalyst synthesis process.

2.3. Physicochemical Characterization

The physicochemical properties of the as-prepared MXene/g-C_3N_4 photocatalysts were studied via several characterization techniques. The crystallinity behavior of the prepared photocatalysts was examined by X-ray diffraction (XRD; PANalytical model: Xpert3 powder) with Cu-Kα radiation. Fourier transform infrared spectroscopy (FTIR) was performed using Shimadzu 8400S within the range of 450 to 4000 cm^{-1} to identify the various functional groups in the as-prepared photocatalysts. The morphological structures of the as-prepared MXene/g-C_3N_4 photocatalysts were examined using HRTEM analysis (120 kV Zeiss Libra 200), FESEM analysis (Zeiss Supra 55VP), and SAP (BET: Micromeritic

ASAP 2000). The bandgap energy (DR-UV-Vis) and the surface chemical properties (XPS) were measured using UV-Vis Carry 100 and Thermoscientific K-alpha, respectively.

2.4. Photocatalytic Degradation Testing

The photocatalytic degradation activities of the synthesized MXene/g-C_3N_4 heterostructure photocatalysts were evaluated by using a prepared methylene blue solution. Firstly, 0.5 g of MXene/g-C_3N_4 sample was mixed with 100 mL of 10 mg/L aqueous methylene blue. The pH of the reaction solution was measured in which was recorded at 8. Then, the solution was left in the dark for one hour in order to achieve the adsorption–desorption equilibrium [4]. Later, the experiment continued by irradiating the solution with a visible light source (500 W halogen lamp) with continuous stirring. The temperature of the photocatalytic reaction was maintained at room temperature by using an external tabletop fan. Subsequently, every 30 min, the methylene blue solution was extracted by using a plastic syringe attached with a 0.45 µm filter. The results were analyzed by using a UV-Vis spectrophotometer (UV-1800, Shimadzu) and the degradation activity of methylene blue solution was studied using the following equation:

$$Degradation\ of\ Methylene\ Blue\ (\%) = \left[\frac{Abs_0 - Abs_F}{Abs_0}\right] \times 100 \quad (1)$$

where Abs_0 and Abs_F are the initial and final absorbance of methylene blue solution at a designated time.

3. Results

3.1. FTIR Analysis

Figure 2 shows the detailed structures of g-C_3N_4, MXene, and the as-synthesized g-C_3N_4/MXene photocatalysts that were characterized by FTIR. Three distinguished characterized peaks were observed. The broad adsorption peaks at 3000–3600 cm^{-1} indicate the existence of the -NH functional group, allowing the N-H stretching vibrations, as well as the termination of OH of the adsorbed hydroxyl species [17,18]. The strong peaks in the region of 1100–1700 cm^{-1} indicate the C-N and C=N in the heterocycles of CN [13,19]. Other than that, the visible peak at 800 cm^{-1} is attributable to the breathing mode of tri-s-triazine [15]. With regard to composites of MXene/g-C_3N_4, the characteristics of the g-C_3N_4 were well preserved as the primary characteristic peaks of g-C_3N_4 were clearly observed. The results show that the growing loading amount of MXene gradually reduced the magnitude of peaks, indicating the reduction of some structures in g-C_3N_4 through the combination of g-C_3N_4 with Ti_3C_2. The addition of larger amounts of MXene facilitated more changes that occurred to the structure of MXene/g-C_3N_4 photocatalyst.

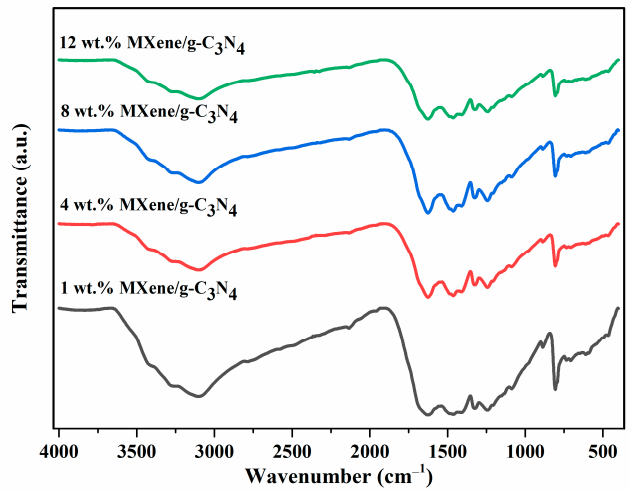

Figure 2. FTIR patterns of the as-prepared MXene/g-C_3N_4 photocatalyst.

3.2. XRD Analysis

The XRD analysis of the g-C_3N_4, MXene, 1 wt.% MXene/g-C_3N_4, 4 wt.% MXene/g-C_3N_4, 8 wt.% MXene/g-C_3N_4, and 12 wt.% MXene/g-C_3N_4 heterostructure photocatalysts were performed in order to examine the crystallinity behavior of the as-developed materials. Figure 3 shows the XRD pattern of MXene, which is in agreement with the previously reported study (JCPDS card No. 52–0975) [20,21]. By comparing the obtained results of the as-synthesized photocatalysts, the most intense peak of MXene, which is commonly observed at 39° of 2θ, disappeared, signifying the disappearance of Al after etching by HF. In this context, the obtained results stipulate that Al managed to be removed and MXene was successfully obtained. Additionally, the (004) peak located at 17.6° of 2θ was monitored to be shifted to the higher angle, indicating an interaction between MXene and g-C_3N_4. Furthermore, the (107) peak observed at 47° of 2θ became stronger as the amount of MXene loading was increased in the formation of the MXene/g-C_3N_4 heterostructure photocatalyst.

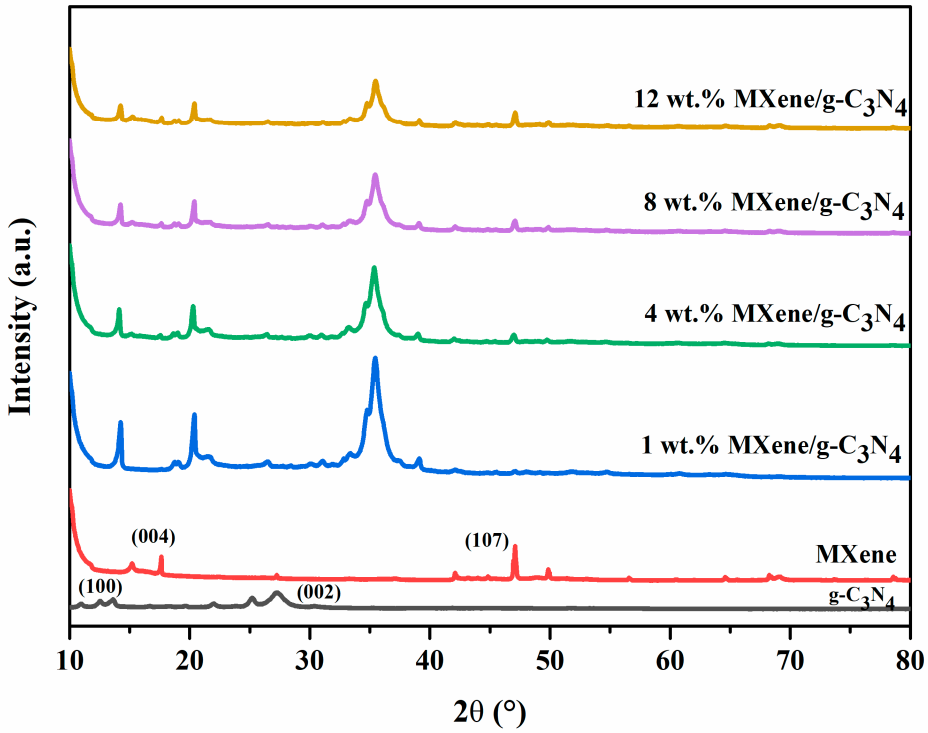

Figure 3. XRD patterns of the as-synthesized MXene/g-C_3N_4 heterostructure photocatalysts.

On the other hand, two different diffraction peaks, located at 12.5° and 27.7° of 2θ, were attributed to g-C_3N_4 footprints (JCPDS card No. 87–1526). The peaks at 27.7° indicate the multilayer π-π stacking of g-C_3N_4, while the peak of 12.5° signifies the in-plane repeated units [22,23]. The XRD patterns of MXene/g-C_3N_4 composites with different amounts of MXene loaded onto the heterostructure sample show almost identical diffraction peaks. Nevertheless, as the amount of MXene loading was increased to 12 wt.%, the peaks located at 12.5°, 13.9°, and 35° of 2θ became weakened. Such occurrences may happen due to the interaction between MXene and g-C_3N_4, which disrupts the aromatic conditions of g-C_3N_4 [13,24]. As such, the obtained XRD patterns of the as-synthesized heterostructure photocatalyst proved the successful loading of MXene onto g-C_3N_4. Furthermore, higher loading of MXene leads to the shift of peak towards a higher angle, indicating stronger interaction of the two different materials, which leads to a further stacking distance of g-C_3N_4.

3.3. Morphological Analysis

Figure 4 represents the FESEM micrograph images of the as-synthesized MXene/g-C_3N_4 heterostructure photocatalysts prepared at different amounts of MXene loadings. The FESEM images demonstrated the successful formation of layered MXene by etching the Ti_3AlC_2 MAX using HF [25]. Generally, the Ti_3AlC_2 structures were made up of an irregular block structure. However, after the etching process with HF, the as-prepared MXene demonstrated an obvious stratification, evincing the successful etching process of aluminum layers. Meanwhile, the presence of a crumple-sheet-like structure in the composite heterostructure photocatalysts is attributed to the morphological structure of the g-C_3N_4 [26,27]. All of the FESEM images displayed the encapsulation and intimate contact between both g-C_3N_4 and MXene, evincing the successful development of the heterostructure system. In addition, as both the g-C_3N_4 and MXene form the 2D nanostructure, intimate contact between each photocatalyst was observed. In light of this, a smooth photocharge carrier transfer was postulated with respect to its well-matched geometrical structure. Thereafter, the issue of the fast recombination of the photocharge carriers within the individual photocatalyst can be mitigated. Moreover, Figure 5 represents the TEM images of the as-synthesized MXene/g-C_3N_4 heterostructure photocatalysts. A typical 2D multilayered structure could be seen from the inset in Figure 5, where the interlayer spacing measured 0.25 nm. The aforesaid interlayer spacing corresponds to the (101) crystal plane of Ti_3C_2 MXene [25,28,29]. After the etching process of Ti_3AlC_2, the structure of Ti_3C_2 MXene with a very small spacing has been produced. Nevertheless, the lattice fringe of the pure g-C_3N_4 photocatalyst was hardly visible, presumably due to the low crystallinity. On a whole, the FESEM and HRTEM analysis verified the successful interfacial contact between both MXene and g-C_3N_4 particles, which will be beneficial for augmenting the photocharge carriers' separation and migration, resulting in an enhancement in the photocatalytic degradation activity.

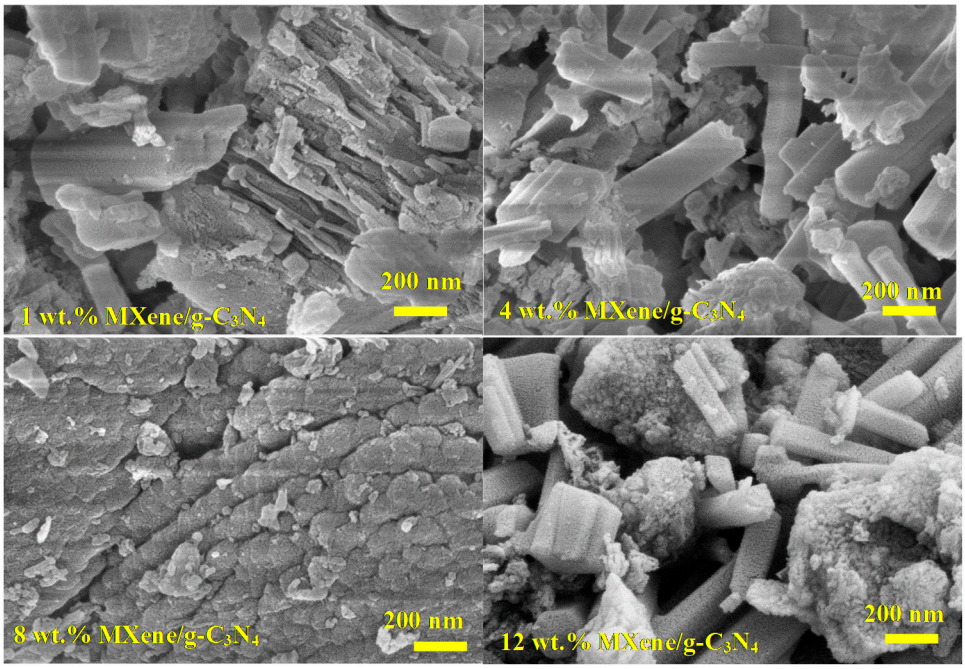

Figure 4. FESEM images of the as-synthesized MXene/g-C_3N_4 heterostructure photocatalysts.

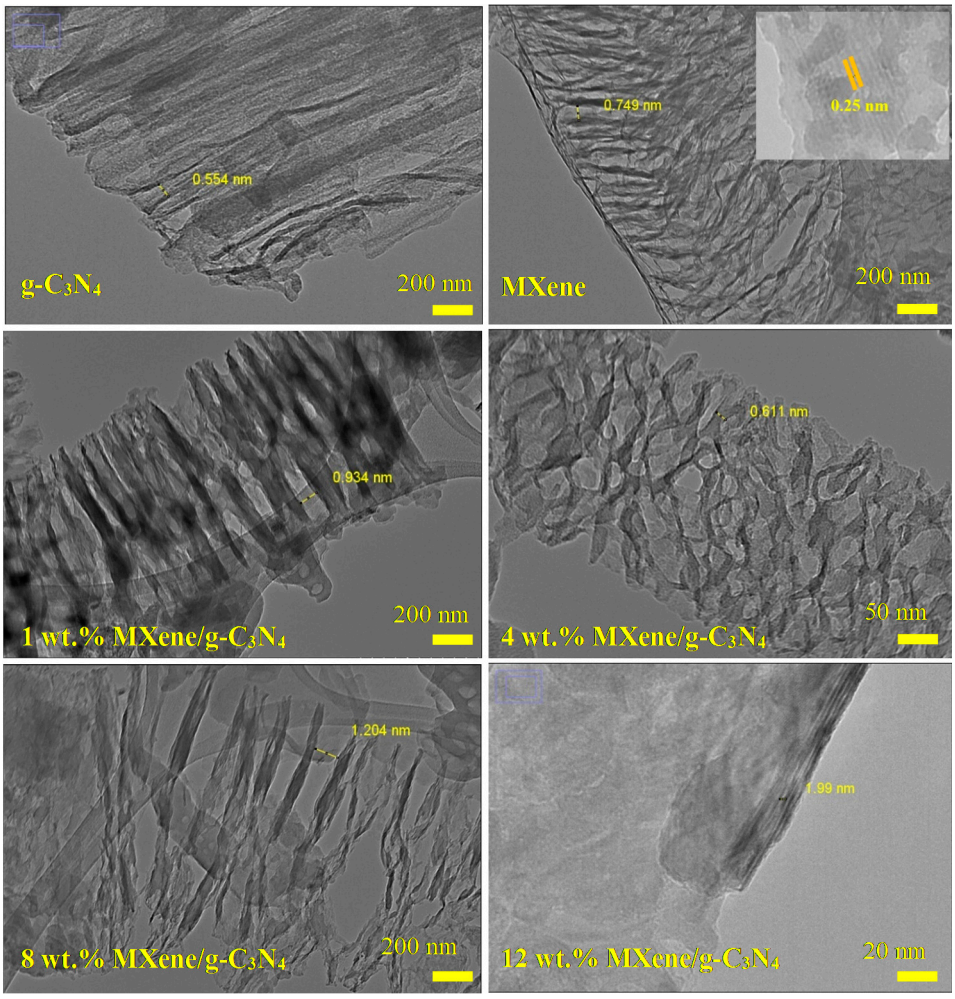

Figure 5. TEM images of the as-synthesized MXene/g-C_3N_4 heterostructure photocatalysts.

3.4. BET Surface Area and Porosity Analysis

The BET specific surface area, pore volume, and pore size analyses of the as-synthesized MXene/g-C_3N_4 heterostructure photocatalysts prepared at different amounts of MXene loadings are summarized in Table 1. It was found that the BET surface areas for the pure g-C_3N_4 and MXene were 4.64 and 6.26 m^2/g, respectively. Upon the formation of the MXene/g-C_3N_4 heterostructure system, the BET surface area was substantially increased to 22.58 m^2/g. Similarly, the pore size and pore volume of the 1 wt.% MXene/g-C_3N_4 heterostructure sample showed significant enhancement, at 0.123 cm^3/g and 21.88 nm, respectively. It is worth mentioning that the high BET surface area, pore size, and pore volume are highly desirable as it is beneficial for improving the photocatalytic degradation activity of the heterostructure photocatalyst. This is explained by the fact that more pollutants can be adsorbed via the high surface area of the designed heterostructure photocatalyst. As such, a higher photocatalytic degradation performance will be achieved via the 1 wt.% MXene/g-C_3N_4 heterostructure sample.

Nevertheless, as the amount of MXene loading was increased up to 12 wt.%, the BET surface area, pore size, and pore volume of the rest of the MXene/g-C_3N_4 heterostructure samples were decreased to 13.70 m^2/g, 0.033 cm^3/g, and 9.535 nm, respectively. The lower textural properties demonstrated by the 12 wt.% MXene/g-C_3N_4 heterostructure sample are highly unfavorable from the photocatalytic viewpoint as this indicates that less available active pore sites will partake in the degradation of methylene blue. Thereafter, a substantial decrease in photocatalytic degradation activity will be monitored. Apart from that, Figure 6 shows that the as-prepared MXene/g-C_3N_4 heterostructure samples possessed a Type IV

adsorption isotherm with an H3 hysteresis pattern. In particular, the observed pattern highlights the mesoporous structure of the as-synthesized MXene/g-C_3N_4 heterostructure samples, whereby pore size ranged from 2–50 nm.

Table 1. BET surface area, pore volume, and pore size of the as-synthesized MXene/g-C_3N_4 heterostructure photocatalysts.

Photocatalyst	BET Surface Area (m^2/g)	Pore Volume (cm^3/g)	Pore Size (nm)
g-C_3N_4	4.64	0.033	28.09
MXene	6.26	0.027	16.96
1 wt.% MXene/g-C_3N_4	22.58	0.123	21.88
4 wt.% MXene/g-C_3N_4	15.66	0.036	9.377
8 wt.% MXene/g-C_3N_4	17.73	0.039	8.826
12 wt.% MXene/g-C_3N_4	13.70	0.033	9.535

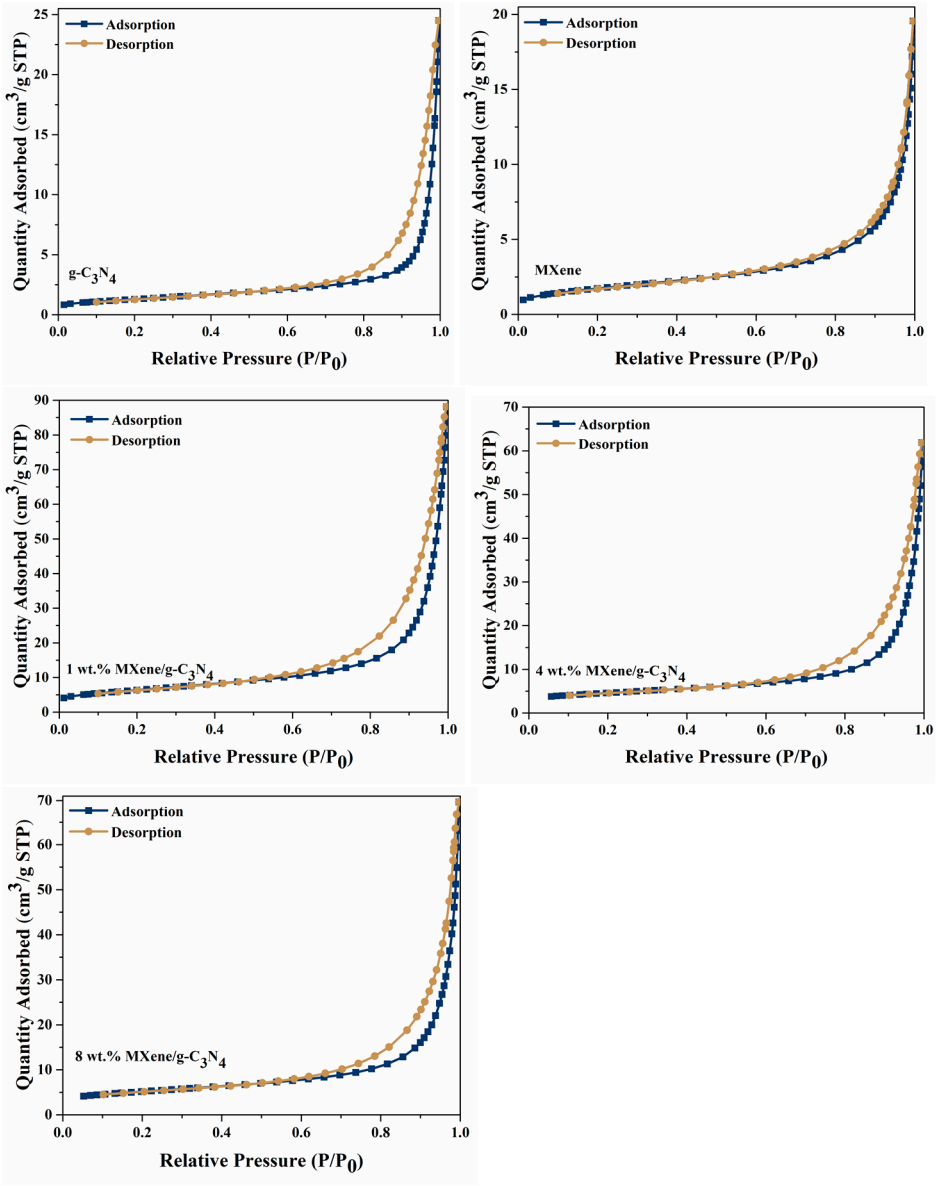

Figure 6. Nitrogen adsorption–desorption isotherms of the as-synthesized MXene/g-C_3N_4 heterostructure photocatalysts.

3.5. Optical Properties

The optical properties of the as-synthesized MXene/g-C_3N_4 heterostructure photocatalysts prepared at different amounts of MXene loadings were examined using UV-Vis diffuse reflectance spectra (DR-UV-Vis). Figure 7a shows that the g-C_3N_4 photocatalyst showed a light absorption capacity within the visible-light region. Similarly, the loading of the MXene onto g-C_3N_4 photocatalyst further narrowed the light absorption capacity with a slight blue shift and red shift in accordance with the amount of MXene loading. In turn, this observation indicates the potential of the photocatalytic light absorption response up to 48% of the total solar light energy. Moreover, as the composite MXene/g-C_3N_4 heterostructure photocatalysts possess a stronger visible-light absorption capacity, the enhancement in photothermal effect could be observed, which would be beneficial in aiding the photocatalytic activity of the aforesaid samples. Following that, Figure 7b illustrates the plotted and estimated bandgap energy using Tauc plot calculation. The bandgap energy of the pure g-C_3N_4 was 2.61 eV. The obtained bandgap energy aligns with several previously reported works on g-C_3N_4 photocatalysts [30,31]. As depicted in Figure 7b, the bandgap energy for the 1 wt.% MXene/g-C_3N_4, 4 wt.% MXene/g-C_3N_4, 8 wt.% MXene/g-C_3N_4, and 12 wt.% MXene/g-C_3N_4 samples were 2.53, 2.09, 2.20 and 2.31 eV, respectively.

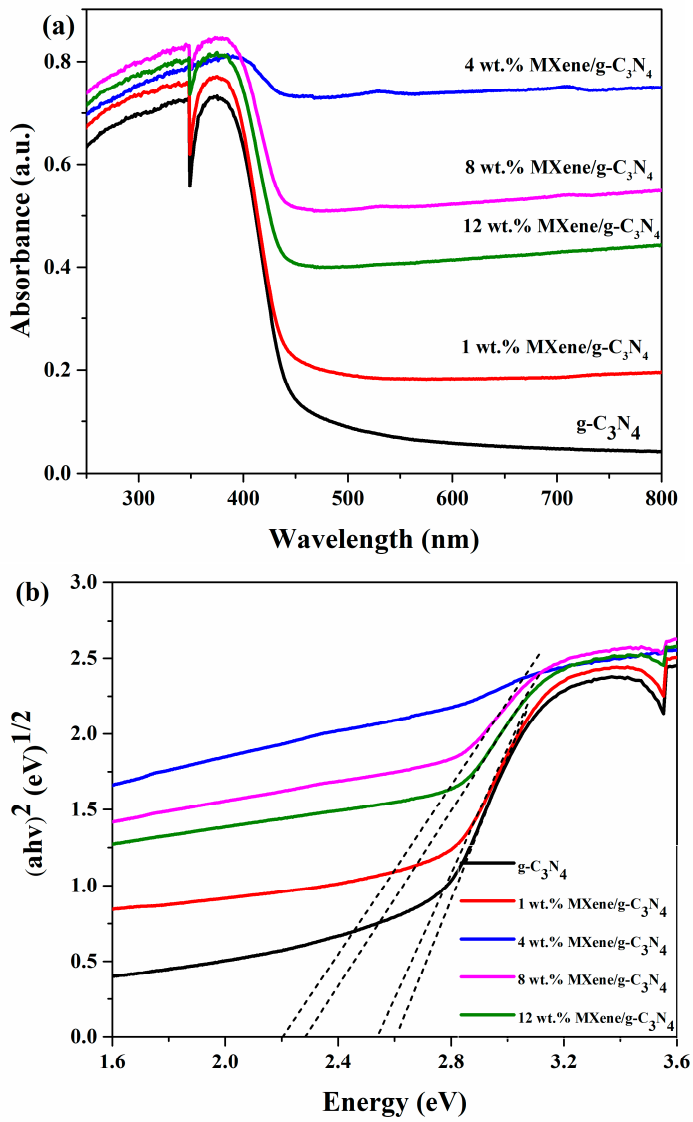

Figure 7. (**a**) UV-Vis diffuse reflection absorption spectra and (**b**) Tauc plots of the as-synthesized MXene/g-C_3N_4 heterostructure photocatalysts.

3.6. XPS Analysis

The elemental and surface chemical properties of the 1 wt.% MXene/g-C_3N_4 heterostructure photocatalyst were examined via XPS analysis. Figure 8 delineates the XPS spectrum of C 1s, Ti 2p, O 1s, and N 1s. As displayed in Figure 8a, three significant peaks were observed in the C 1s spectrum. Accordingly, the observed peaks, located at 281.5, 284.8, and 286.3 eV, confirm the presence of the C-Ti, C-C, and C-O bonds, respectively, in the 1 wt.% MXene/g-C_3N_4 heterostructure photocatalyst [13,24]. The reason behind the observed peaks is the presence of the g-C_3N_4 particles in the heterostructure sample. Moreover, the peaks located at 284.8 eV are attributable to the C-C adventitious carbon that was used as the energy reference in fitting the XPS spectrum of the 1 wt.% MXene/g-C_3N_4 heterostructure photocatalyst.

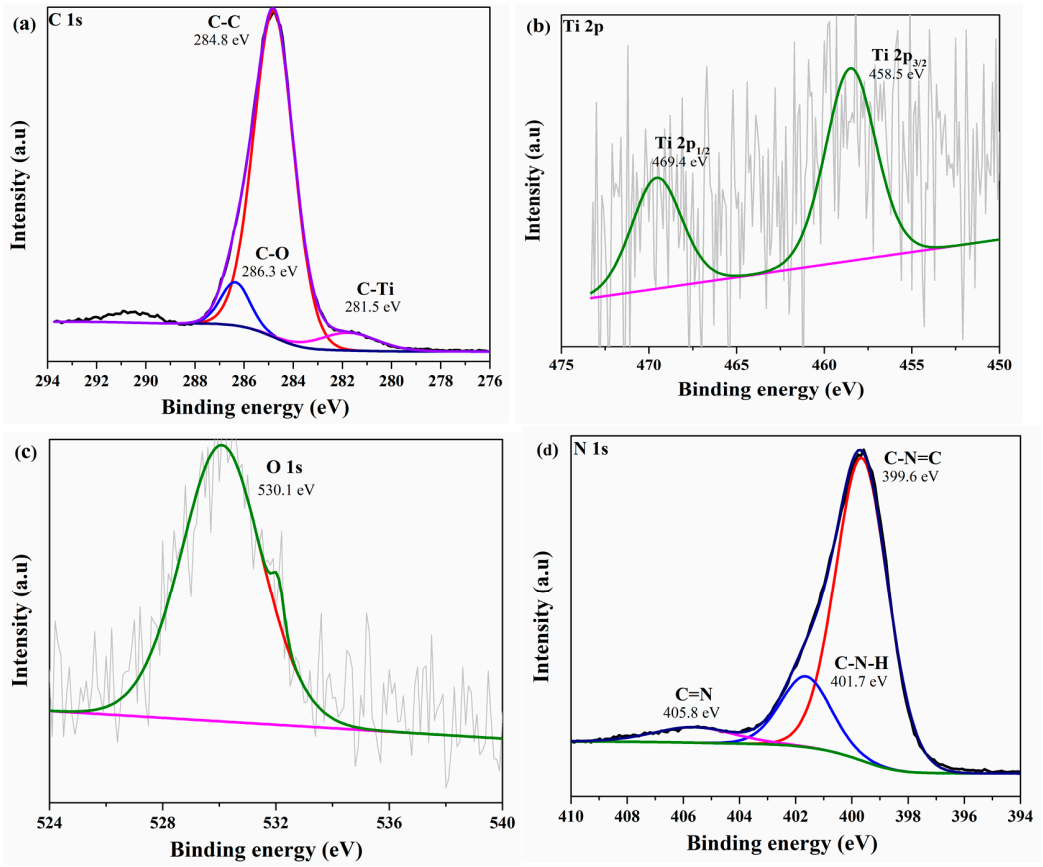

Figure 8. (**a**) C 1s, (**b**) Ti 2p, (**c**) O 1s, and (**d**) N 1s high-resolution XPS spectra of the as-synthesized 1 wt.% MXene/g-C_3N_4 heterostructure photocatalyst.

Additionally, Figure 8b shows the Ti 2p spectrum, composed of two deconvoluted peaks located at 458.5 and 469.4 eV. The observed peaks were well-matched with the Ti $2p_{3/2}$ and Ti $2p_{1/2}$ of the Ti-C bond [21,32,33]. The aforesaid deconvoluted peaks demonstrated a strong peak, which was presumably due to the potential of the oxidation on the surface of the MXene, which later converted into Ti-O bonds. Furthermore, the O 1s energy spectrum in Figure 8c exhibited a peak located at 530.1 eV, which can be ascribed to the absorbed hydroxyl group. Apart from that, Figure 8d shows three peaks, deconvoluted at 399.6, 401.7, and 405.8 eV. The three peaks observed coincided well with the C-N=C, C-N-H, and C=N bonds, which originated from the parental g-C_3N_4 and MXene particles [34,35]. It is worthwhile to note that all of the XPS peaks showed a shift to higher and lower binding energies in comparison to the standard parental g-C_3N_4 and MXene peaks. The shifting phenomenon of the observed peaks signifies the presence of interfacial photocharge carriers

transfer within the 1 wt.% MXene/g-C_3N_4 heterostructure photocatalyst, which will be beneficial for the photocatalytic degradation activity.

3.7. Photocatalytic Degradation Performance Testing

Figure 9 shows the results of MB degradation, with different compositions of the as-synthesized MXene/g-C_3N_4 heterostructure photocatalyst. For the first hour of investigation, the degradation was commenced under dark conditions and further continued for another 3 h with the presence of light irradiation. In this study, the photocatalytic degradation of MB was determined at 664 nm due to the absence of blue shift of the main peak of MB during the photocatalytic experiment [36].

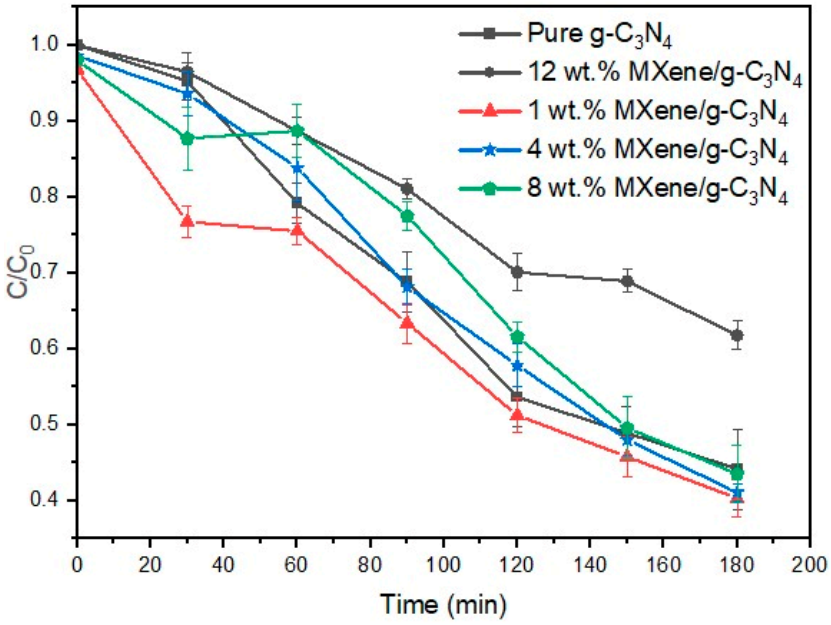

Figure 9. Photocatalytic degradation of methylene blue using MXene/g-C_3N_4 heterostructure photocatalysts prepared with different amounts of MXene loading.

The efficiency for degradation of the as-prepared samples was calculated by using the equation stated in Section 2.4. The photocatalytic activity of the as-synthesized MXene/g-C_3N_4 heterostructure photocatalyst indicates that the performance of the heterostructure samples was ordered as 1 wt.% MXene/g-C_3N_4 sample > 4 wt.% MXene/g-C_3N_4 sample > 8 wt.% MXene/g-C_3N_4 sample > pure g-C_3N_4 sample > 12 wt.% MXene/g-C_3N_4 sample. In this regard, the 1 wt.% MXene/g-C_3N_4 sample exhibited the highest degradation activity within 180 min. This is explained by the fact that the aforesaid sample possessed a higher BET surface area, pore size, and pore volume, which was beneficial for improving the photocatalytic reaction. In light of this enhancement, more methylene blue compounds can be adsorbed via the 1 wt.% MXene/g-C_3N_4 sample, whereby more active radicals can be generated to further degrade the methylene blue molecules and eventually attain the complete removal of the recalcitrant pollutant.

Furthermore, the narrow bandgap energy of this heterostructure sample is highly favorable for the photocatalytic reaction as more light can be absorbed, thus generating more photocharge carriers to participate in the photocatalytic reaction. As mentioned earlier, the intimate contact between g-C_3N_4 and MXene particles, evident from the FESEM analysis, firmly implies that the aforesaid heterostructure system allows mobility of the smooth photocharge carriers, which significantly hindered the potential of the photocharge carriers' recombination. In turn, this phenomenon allows the MXene/g-C_3N_4 heterostructure photocatalyst to perform better than the pure g-C_3N_4. Nonetheless, a reverse scenario was demonstrated by the 12 wt.% MXene/g-C_3N_4 sample. The overloading of the MXene onto

the g-C_3N_4 photocatalyst leads to a detrimental photocatalytic performance. This is consistent with the SAP analysis in Section 3.4, whereby the BET surface area, pore size, and pore volume substantially decreased as the amount of MXene loading was increased [2,37,38].

3.8. Possible Route for Photodegradation of Methylene Blue over MXene/g-C_3N_4 Heterostructure Photocatalyst

Figure 10 demonstrates the active site radical trapping experiments in order to verify the role of relative active species that contributed during the photocatalytic degradation of methylene blue using the 1 wt.% MXene/g-C_3N_4 sample. The radical trapping experiment was conducted in the similar protocols used in Section 2.4. In this experiment, the methanol, 2-propanol, and $AgNO_3$ were used as a scavengers for $\bullet O_2^-$, •OH, and e^- species, respectively. In view of this radical trapping experiment, it was found that the addition of $AgNO_3$ as an electron scavenger had a substantial effect on the photocatalytic activity of the 1 wt.% MXene/g-C_3N_4 sample. Meanwhile, the addition of methanol and 2-propanol had mediocre effects on the activity of the 1 wt.% MXene/g-C_3N_4 sample. By confirming the active sites contributing to the photocatalytic reaction, the electron is likely to take a major role in degrading the methylene blue compounds, whereby the $\bullet O_2^-$ and •OH radicals further support the degradation process. Subsequently, the active radicals will attack the positive carbon compounds of the methylene blue, consecutively degrading methylene blue into biodegradable by-products that can be adsorbed by the designed photocatalyst [39]. Then, the initial compound of methylene blue can break into smaller and more decomposable oxidation by-products, which are relatively less toxic and even less harmless compared to their initial compounds. The intermediates develop hydroxylation by-products and are later mineralized into CO_2 and H_2O after being attacked by the active site radicals.

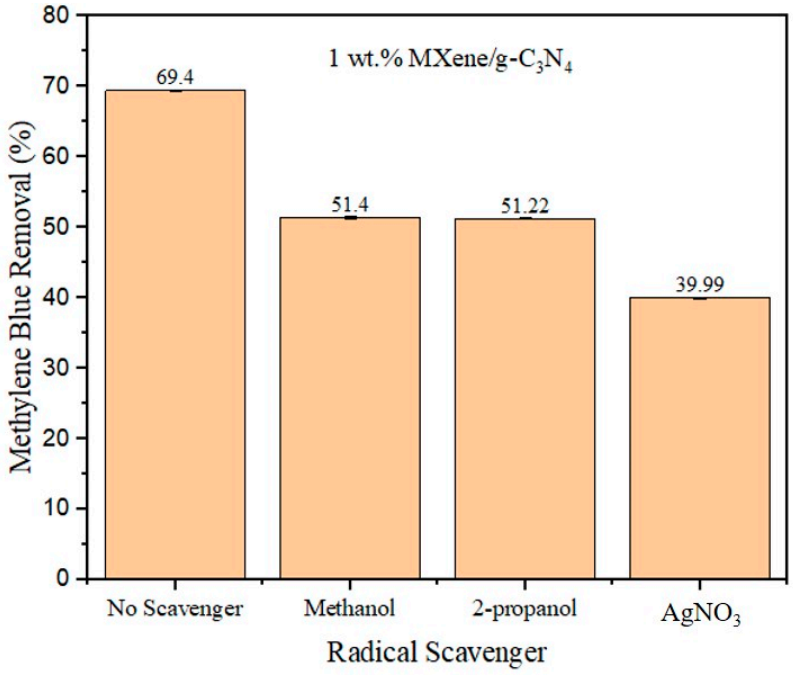

Figure 10. Active sites radical trapping studies on the as-synthesized 1 wt.% MXene/g-C_3N_4 heterostructure photocatalysts.

Based on the abovementioned analysis, the mechanism of the degradation of methylene blue via the 1 wt.% MXene/g-C_3N_4 photocatalyst was postulated and calculated as

illustrated in Figure 11. The valence band (VB) and conduction band (CB) of the aforementioned photocatalyst were calculated based on the following equation:

$$E_{VB} = X - E^e + \frac{1}{2} E_g \quad (2)$$

$$E_{CB} = E_{VB} - E_g \quad (3)$$

where the E_{VB}, E_{CB}, X, and E_g correspond to the valence band potential, conduction band potential, absolute electronegativity, and bandgap energy, respectively. More detailed explanations on the abovementioned equation have been explained in the previously reported work [8]. The value for the E^e, X, and E_g were 4.5, 4.64, and 2.61 eV, respectively. Thereafter, the calculated E_{VB} and E_{CB} of the g-C_3N_4 were 1.445 and −1.165 eV, respectively. Thereafter, under light illumination, the g-C_3N_4 photocatalyst absorbed the photon energy, thus initiating the generation of the electron and hole to partake in the photocatalytic reaction. As the MXene is not a visible-light absorption material, the MXene acts as an electron acceptor with respect to its well-matched band edge position, thus allowing the electrons at the conduction band of g-C_3N_4 to quickly transfer to MXene (E_F = −0.53 eV vs. NHE). Subsequently, the photoexcited electrons further attacked the methylene blue compound and further degraded it into intermediate by-products. In addition, as the E_F of MXene is more negative than the standard $O_2/\bullet O_2^-$, the superoxide radicals ($\bullet O_2^-$) are readily produced upon excitation of electrons and further assist the degradation of methylene blue. On the other hand, the holes at the valence band of g-C_3N_4 can further oxidize to produce the •OH radicals, thus attacking and degrading the methylene compounds.

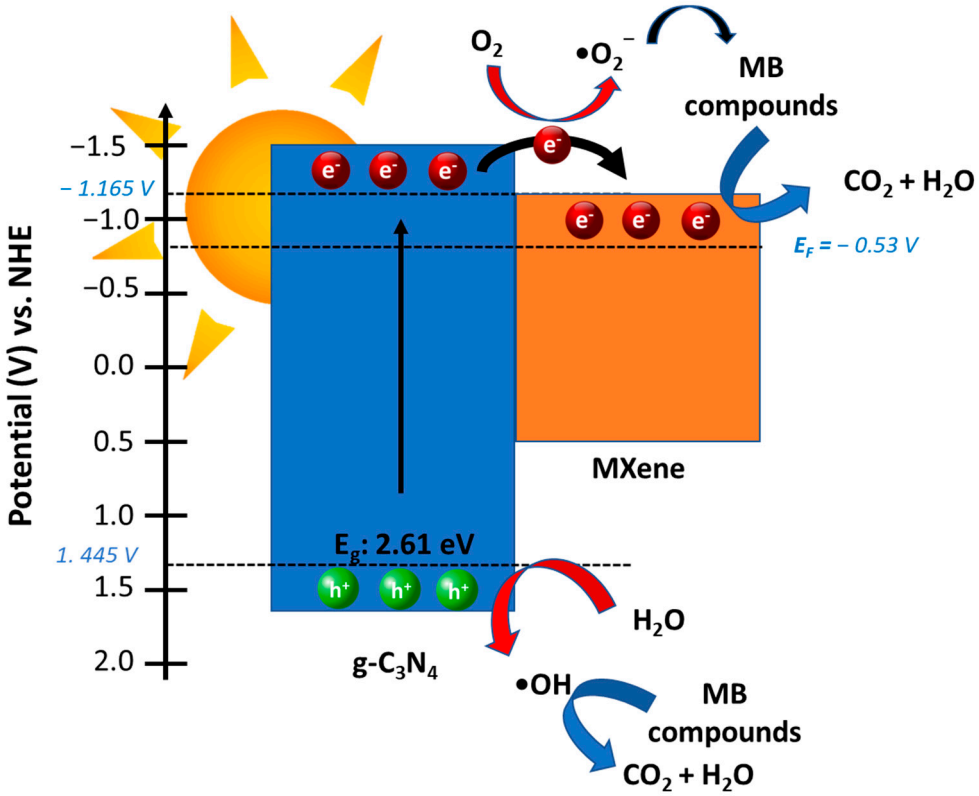

Figure 11. The possible degradation mechanism for photocatalyst reaction of MXene/g-C_3N_4 heterostructure photocatalyst.

4. Conclusions

In conclusion, the work presented here demonstrated that an excellent photocatalytic degradation of methylene blue can be achieved via MXene/g-C_3N_4 heterostructure photocatalysts. The designed 1 wt.% MXene/g-C_3N_4 heterostructure photocatalyst exhibited

the best photocatalytic performance within 180 min. Undoubtedly, the high BET surface area, stronger XRD crystallinity structures, and narrower bandgap energy play a vital role in improving the photocatalytic activity of the aforesaid heterostructure photocatalyst. Furthermore, it was found that the e^- was confirmed to play a major role in the studied photocatalytic reaction. This enhancement originated from the critical roles of MXene that helped to impede the recombination of the photocharge carriers and, thus, further augmented the photocatalytic reaction. On a whole, this work presents MXene as a new alternative that will further improve charge separation and transportation, as well as further promotes the degradation of dye in wastewater under solar irradiation.

Author Contributions: M.S.I.N.: writing original draft, formal analysis, investigation; M.F.R.S.: formal analysis, writing—review and editing; A.A.T.: funding acquisition; S.S.: supervision, funding acquisition, review and editing. All authors have read and agreed to the published version of the manuscript.

Funding: This work was funded by Yayasan Universiti Teknologi PETRONAS (015LC0-357), Fundamental Research Grant Scheme, FRGS-MOHE (Ref no: FRGS/1/2020/TK0/UTP/02/22) and Engineering and Physical Science Research Council, UK (EPSRC under research grant No. EP/V049046/1 and EP/T025875/1).

Institutional Review Board Statement: Not applicable.

Informed Consent Statement: Not applicable.

Data Availability Statement: Not applicable.

Acknowledgments: The authors would like to express their appreciation to the Chemical Engineering Department of Universiti Teknologi PETRONAS and Centre of Innovative Nanostructures and Nanodevices (COINN) for the financial and laboratory support. A.A. Tahir also is thankful to the Engineering and Physical Science Research Council, UK for financial support.

Conflicts of Interest: The authors declare that they have no conflict of interest.

References

1. Desore, A.; Narula, S.A. An overview on corporate response towards sustainability issues in textile industry. *Environ. Dev. Sustain.* **2018**, *20*, 1439–1459. [CrossRef]
2. Kurniawan, T.A.; Mengting, Z.; Fu, D.; Yeap, S.K.; Othman, M.H.D.; Avtar, R.; Ouyang, T. Functionalizing TiO_2 with graphene oxide for enhancing photocatalytic degradation of methylene blue (MB) in contaminated wastewater. *J. Environ. Manag.* **2020**, *270*, 110871. [CrossRef]
3. Kusiak-Nejman, E.; Wanag, A.; Kapica-Kozar, J.; Kowalczyk, Ł.; Zgrzebnicki, M.; Tryba, B.; Przepiórski, J.; Morawski, A.W. Methylene blue decomposition on TiO_2/reduced graphene oxide hybrid photocatalysts obtained by a two-step hydrothermal and calcination synthesis. *Catal. Today* **2020**, *357*, 630–637. [CrossRef]
4. Samsudin, M.F.R.; Frebillot, C.; Kaddoury, Y.; Sufian, S.; Ong, W.J. Bifunctional Z-Scheme Ag/$AgVO_3$/g-C_3N_4 photocatalysts for expired ciprofloxacin degradation and hydrogen production from natural rainwater without using scavengers. *J. Environ. Manag.* **2020**, *270*, 110803. [CrossRef] [PubMed]
5. Zhang, C.; Li, Y.; Shuai, D.; Shen, Y.; Xiong, W.; Wang, L. Graphitic carbon nitride (g-C_3N_4)-based photocatalysts for water disinfection and microbial control: A review. *Chemosphere* **2019**, *214*, 462–479. [CrossRef] [PubMed]
6. Matafonova, G.; Batoev, V. Recent advances in application of UV light-emitting diodes for degrading organic pollutants in water through advanced oxidation processes: A review. *Water Res.* **2018**, *132*, 177–189. [CrossRef] [PubMed]
7. Raizada, P.; Sudhaik, A.; Singh, P. Photocatalytic water decontamination using graphene and ZnO coupled photocatalysts: A review. *Mater. Sci. Energy Technol.* **2019**, *2*, 509–525. [CrossRef]
8. Samsudin, M.F.R.; Bacho, N.; Sufian, S.; Ng, Y.H. Photocatalytic degradation of phenol wastewater over Z-scheme g-C_3N_4/CNT/$BiVO_4$ heterostructure photocatalyst under solar light irradiation. *J. Mol. Liq.* **2018**, *277*, 977–988. [CrossRef]
9. Malik, R.; Tomer, V.K. State-of-the-art review of morphological advancements in graphitic carbon nitride (g-CN) for sustainable hydrogen production. *Renew. Sustain. Energy Rev.* **2021**, *135*, 110235. [CrossRef]
10. Ni, Y.; Wang, R.; Zhang, W.; Shi, S.; Zhu, W.; Liu, M.; Yang, C.; Xie, X.; Wang, J. Graphitic carbon nitride (g-C_3N_4)-based nanostructured materials for photodynamic inactivation: Synthesis, efficacy and mechanism. *Chem. Eng. J.* **2021**, *404*, 126528. [CrossRef]
11. Huang, D.; Yan, X.; Yan, M.; Zeng, G.; Zhou, C.; Wan, J.; Cheng, M.; Xue, W. Graphitic Carbon Nitride-Based Heterojunction Photoactive Nanocomposites: Applications and Mechanism Insight. *ACS Appl. Mater. Interfaces* **2018**, *10*, 21035–21055. [CrossRef] [PubMed]

12. Li, K.; Zhang, S.; Li, Y.; Fan, J.; Lv, K. MXenes as noble-metal-alternative co-catalysts in photocatalysis. *Chin. J. Catal.* **2020**, *42*, 3–14. [CrossRef]
13. Xu, H.; Xiao, R.; Huang, J.; Jiang, Y.; Zhao, C.; Yang, X. In situ construction of protonated g-C_3N_4/Ti_3C_2 MXene Schottky heterojunctions for efficient photocatalytic hydrogen production. *Chin. J. Catal.* **2021**, *42*, 107–114. [CrossRef]
14. Pang, J.; Mendes, R.G.; Bachmatiuk, A.; Zhao, L.; Ta, H.Q.; Gemming, T.; Liu, H.; Liu, Z.; Rummeli, M.H. Applications of 2D MXenes in energy conversion and storage systems. *Chem. Soc. Rev.* **2019**, *48*, 72–133. [CrossRef]
15. Samsudin, M.F.R.; Ullah, H.; Tahir, A.A.; Li, X.; Ng, Y.H.; Sufian, S. Superior photoelectrocatalytic performance of ternary structural $BiVO_4$/GQD/g-C_3N_4 heterojunction. *J. Colloid Interface Sci.* **2021**, *586*, 785–796. [CrossRef] [PubMed]
16. Sun, Y.; Jin, D.; Sun, Y.; Meng, X.; Gao, Y.; Dall'Agnese, Y.; Chen, G.; Wang, X.F. G-C_3N_4/$Ti_3C_2T_X$ (MXenes) composite with oxidized surface groups for efficient photocatalytic hydrogen evolution. *J. Mater. Chem. A* **2018**, *6*, 9124–9131. [CrossRef]
17. Li, H.; Tian, H.; Wang, X.; Pi, M.; Wei, S.; Zhu, H.; Zhang, D.; Chen, S. Self-Coupled g-C_3N_4 van der Waals Heterojunctions for Enhanced Photocatalytic Hydrogen Production. *ACS Appl. Energy Mater.* **2019**, *2*, 4692–4699. [CrossRef]
18. Zhang, L.; Hao, X.; Li, Y.; Jin, Z. Performance of WO_3/g-C_3N_4 heterojunction composite boosting with NiS for photocatalytic hydrogen evolution. *Appl. Surf. Sci.* **2020**, *499*, 143862. [CrossRef]
19. Jing, H.; Ou, R.; Yu, H.; Zhao, Y.; Lu, Y.; Huo, M.; Huo, H.; Wang, X. Engineering of g-C_3N_4 nanoparticles/WO_3 hollow microspheres photocatalyst with Z-scheme heterostructure for boosting tetracycline hydrochloride degradation. *Sep. Purif. Technol.* **2021**, *255*, 117646. [CrossRef]
20. Ta, Q.T.H.; Tran, N.M.; Tri, N.N.; Sreedhar, A.; Noh, J.S. Highly surface-active Si-doped TiO_2/$Ti_3C_2T_x$ heterostructure for gas sensing and photodegradation of toxic matters. *Chem. Eng. J.* **2021**, *425*, 131437. [CrossRef]
21. Huang, K.; Li, C.; Wang, L.; Wang, W.; Meng, X. Layered Ti_3C_2 MXene and silver co-modified g-C_3N_4 with enhanced visible light-driven photocatalytic activity. *Chem. Eng. J.* **2021**, *425*, 131493. [CrossRef]
22. Mohamed, N.A.; Safaei, J.; Ismail, A.F.; Khalid, M.N.; Mohd Jailani, M.F.A.; Noh, M.F.M.; Arzaee, N.A.; Zhou, D.; Sagu, J.S.; Teridi, M.A.M. Boosting photocatalytic activities of BiVO4 by creation of g-C_3N_4/ZnO@$BiVO_4$ Heterojunction. *Mater. Res. Bull.* **2020**, *125*, 110779. [CrossRef]
23. Wang, S.; Chen, L.; Zhao, X.; Zhang, J.; Ao, Z.; Liu, W.; Wu, H.; Shi, L.; Yin, Y.; Xu, X.; et al. Efficient photocatalytic overall water splitting on metal-free 1D SWCNT/2D ultrathin C_3N_4 heterojunctions via novel non-resonant plasmonic effect. *Appl. Catal. B Environ.* **2020**, *278*, 119312. [CrossRef]
24. Han, X.; An, L.; Hu, Y.; Li, Y.; Hou, C.; Wang, H.; Zhang, Q. Ti_3C_2 MXene-derived carbon-doped TiO_2 coupled with g-C_3N_4 as the visible-light photocatalysts for photocatalytic H_2 generation. *Appl. Catal. B Environ.* **2020**, *265*, 118539. [CrossRef]
25. Cao, B.; Wan, S.; Wang, Y.; Guo, H.; Ou, M.; Zhong, Q. Highly-efficient visible-light-driven photocatalytic H_2 evolution integrated with microplastic degradation over MXene/ZnxCd1-xS photocatalyst. *J. Colloid Interface Sci.* **2022**, *605*, 311–319. [CrossRef] [PubMed]
26. Zhou, Y.; Zhou, L.; Ni, C.; He, E.; Yu, L.; Li, X. 3D/2D MOF-derived $CoCeO_x$/g-C_3N_4 Z-scheme heterojunction for visible light photocatalysis: Hydrogen production and degradation of carbamazepine. *J. Alloys Compd.* **2022**, *890*, 161786. [CrossRef]
27. Manikandan, V.S.; Harish, S.; Archana, J.; Navaneethan, M. Fabrication of novel hybrid Z-Scheme WO_3@g-C_3N_4@MWCNT nanostructure for photocatalytic degradation of tetracycline and the evaluation of antimicrobial activity. *Chemosphere* **2022**, *287*, 132050. [CrossRef] [PubMed]
28. Thirumal, V.; Yuvakkumar, R.; Kumar, P.S.; Ravi, G.; Keerthana, S.P.; Velauthapillai, D. Facile single-step synthesis of MXene@CNTs hybrid nanocomposite by CVD method to remove hazardous pollutants. *Chemosphere* **2022**, *286*, 131733. [CrossRef] [PubMed]
29. Ma, Y.; Xu, D.; Chen, W.; Tang, Y.; Wang, X.; Li, L.; Wang, J. Oxygen-vacancy-embedded 2D/2D NiFe-LDH/MXene Schottky heterojunction for boosted photodegradation of norfloxacin. *Appl. Surf. Sci.* **2021**, *572*, 151432. [CrossRef]
30. Samsudin, M.F.R.; Ullah, H.; Bashiri, R.; Mohamed, N.M.; Sufian, S.; Ng, Y.H. Experimental and DFT Insights on Microflower g-C_3N_4/$BiVO_4$ Photocatalyst for Enhanced Photoelectrochemical Hydrogen Generation from Lake water. *ACS Sustain. Chem. Eng.* **2020**, *8*, 9393–9403. [CrossRef]
31. Tan, H.L.; Du, A.; Amal, R.; Ng, Y.H. Decorating platinum on nitrogen-doped graphene sheets: Control of the platinum particle size distribution for improved photocatalytic H_2 generation. *Chem. Eng. Sci.* **2018**, *194*, 85–93. [CrossRef]
32. Liu, W.; Sun, M.; Ding, Z.; Gao, B.; Ding, W. Ti_3C_2 MXene embellished g-C_3N_4 nanosheets for improving photocatalytic redox capacity. *J. Alloys Compd.* **2021**, *877*, 160223. [CrossRef]
33. Liu, D.; Li, C.; Ge, J.; Zhao, C.; Zhao, Q.; Zhang, F.; Ni, T.; Wu, W. 3D interconnected g-C_3N_4 hybridized with 2D Ti_3C_2 MXene nanosheets for enhancing visible light photocatalytic hydrogen evolution and dye contaminant elimination. *Appl. Surf. Sci.* **2021**, *579*, 152180. [CrossRef]
34. Zhou, Y.; Yu, M.; Zhan, R.; Wang, X.; Peng, G.; Niu, J. Ti_3C_2 MXene-induced interface electron separation in g-C_3N_4/Ti_3C_2 MXene/$MoSe_2$ Z-scheme heterojunction for enhancing visible light-irradiated enoxacin degradation. *Sep. Purif. Technol.* **2021**, *275*, 119194. [CrossRef]
35. Liu, N.; Lu, N.; Su, Y.; Wang, P.; Quan, X. Fabrication of g-C_3N_4/Ti_3C_2 composite and its visible-light photocatalytic capability for ciprofloxacin degradation. *Sep. Purif. Technol.* **2019**, *211*, 782–789. [CrossRef]
36. Chang, F.; Xie, Y.; Li, C.; Chen, J.; Luo, J.; Hu, X.; Shen, J. A facile modification of g-C_3N_4 with enhanced photocatalytic activity for degradation of methylene blue. *Appl. Surf. Sci.* **2013**, *280*, 967–974. [CrossRef]

37. Regmi, C.; Kshetri, Y.K.; Ray, S.K.; Pandey, R.P.; Lee, S.W. Utilization of visible to NIR light energy by Yb^{+3}, Er^{+3} and Tm^{+3} doped $BiVO_4$ for the photocatalytic degradation of methylene blue. *Appl. Surf. Sci.* **2017**, *392*, 61–70. [CrossRef]
38. Łęcki, T.; Zarębska, K.; Sobczak, K.; Skompska, M. Photocatalytic degradation of 4-chlorophenol with the use of $FTO/TiO_2/SrTiO_3$ composite prepared by microwave-assisted hydrothermal method. *Appl. Surf. Sci.* **2019**, *470*, 991–1002. [CrossRef]
39. Samsudin, M.F.R.; Sufian, S.; Bashiri, R.; Mohamed, N.M.; Ramli, R.M. Synergistic effects of pH and calcination temperature on enhancing photodegradation performance of m-$BiVO_4$. *J. Taiwan Inst. Chem. Eng.* **2017**, *81*, 305–315. [CrossRef]